NUCL SCI TECH (2018) 29:179
https://doi.org/10.1007/s41365-018-0520-z

Search for the chiral magnetic effect in heavy ion collisions

Fu-Qiang Wang[1,2] · **Jie Zhao**[2]

Received: 15 September 2018 / Revised: 2 November 2018 / Accepted: 10 November 2018 / Published online: 23 November 2018

Abstract Quark interactions with topological gluon fields in quantum chromodynamics can yield local $\mathcal{P}$ and $\mathcal{CP}$ violations that could explain the matter–antimatter asymmetry in our universe. Effects of $\mathcal{P}$ and $\mathcal{CP}$ violations can lead to charge separation under a strong magnetic field, a phenomenon called the chiral magnetic effect (CME). Early measurements of the CME-induced charge separation in heavy ion collisions are dominated by physics backgrounds. This report discusses the recent innovative efforts in eliminating those backgrounds, namely by event-shape engineering, invariant mass dependence, and reaction and participant plane comparison. The background-free CME measurements using these novel methods are presented.

Keywords Heavy ion collisions · Chiral magnetic effect · Azimuthal correlator · Flow background · Invariant mass · Reaction plane · Participant plane

This work was supported in part by the National Natural Science Foundation of China (No. 11747312) and the U.S. Department of Energy (No. de-sc0012910).

✉ Fu-Qiang Wang
fqwang@zjhu.edu.cn

[1] School of Science, Huzhou University, Huzhou 313000, China

[2] Department of Physics and Astronomy, Purdue University, West Lafayette, IN 47907, USA

1 Introduction and physics motivation

Our universe started from the Big Bang singularity with equal matter and antimatter [1]; however, it is dominated by matter today. This matter–antimatter asymmetry is caused by the charge conjugation parity ($\mathcal{CP}$) violation, and a slight difference in the physical laws governing matter and antimatter [2, 3]. $\mathcal{CP}$ is violated in the weak interaction; however, the magnitude of the violation is too small to explain the present matter–antimatter asymmetry [4]. $\mathcal{CP}$ violation in the strong interaction of the early universe is required to explain this. $\mathcal{CP}$ violation is not prohibited in the strong interaction, but it has not been observed experimentally. This is called the strong $\mathcal{CP}$ problem [5], one of the remaining problems in physics. The problem can be solved if the $\mathcal{CP}$ symmetry is violated in local metastable domains of topological gluon fields with non-zero topological charges (winding numbers) because of vacuum fluctuations in quantum chromodynamics (QCD) [6–9]. The topological charge, Q_{W}, is proportional to the integral of the scalar product of the gluon (color) electric and magnetic fields over the local domain. Interactions with those topological gluon fields change the helicities of the quarks, thereby causing an imbalance between the left- and right-handed quarks, $Q_{\mathrm{W}} = N_{\mathrm{L}} - N_{\mathrm{R}} \neq 0$, or a local parity ($\mathcal{P}$) violation [9–11]. Such an imbalance can exhibit experimental consequences if submerged in a sufficiently strong magnetic field ($\vec{B}$). The quark spins will be locked, either parallel or anti-parallel to the magnetic field direction, depending on the quark charge. This would result in an experimentally observable charge separation in the final-state hadrons that are products of quark hadronization. This charge separation phenomenon is called the chiral magnetic effect (CME) [12]; see the illustration in Fig. 1.

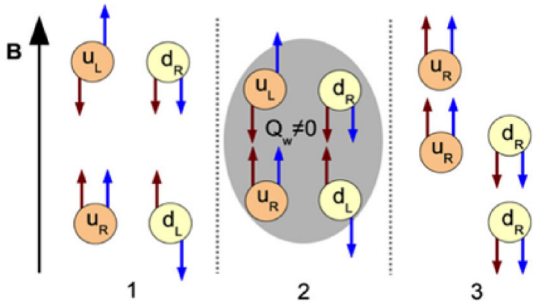

Fig. 1 (Color online) Illustration of the CME. The red arrows denote the direction of momentum, the blue arrows the spin of the quarks. (1) Initially, there were as many left-handed as right-handed quarks. Owing to the strong magnetic field, the up and down quarks are in the lowest Landau level and can only move along the magnetic field. (2) The quarks interact with a topological gluon field with nonzero Q_w, converting left-handed quarks into right-handed ones (in this case $Q_w < 0$) by reversing the momentum direction. (3) The right-handed up quarks will move upward, and the right-handed down quarks will move downward, resulting in a charge separation. From Ref. [11]

Relativistic heavy ion collisions provide an ideal environment for the realization of the CME, as illustrated in Fig. 2. The magnetic field produced by the fast-moving spectator protons in the early times of Au + Au collisions at BNL's Relativistic Heavy Ion Collider (RHIC) is of the order of $B \sim 10^{15}$ Tesla; $eB \sim 0.3m_\pi^2$, where m_π is the pion mass [10–13]. The Landau energy $eB/m_q \sim 1$ GeV is much larger than the typical transverse momenta of the quarks (or the system temperature); therefore, they are locked in the lowest Landau level. Here, $m_q \sim$ of a few MeV are the light quark masses under the approximate chiral symmetry, which is broken spontaneously under normal conditions but is likely restored in relativistic heavy ion collisions where the relevant degrees of freedom are current quarks and gluons [14–18]. The time variation of the magnetic field is less well understood; it can quickly die off with time when the relativistic nuclei pass by quickly, or it could sustain for a relatively long time in a conducting quark–gluon plasma produced in those collisions [19, 20]. Therefore, even if the physics of the CME is correct, its observation is not guaranteed. Meanwhile, an observation of the CME-induced charge separation would confirm several fundamental properties of QCD and solve the long-standing strong $\mathcal{CP}$ problem. It is therefore of paramount importance.

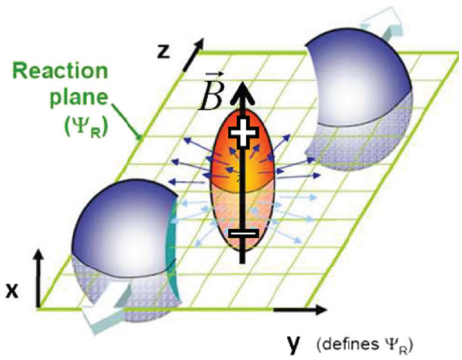

Fig. 2 (Color online) Illustration of a noncentral heavy ion collision, where the overlap participant region is an ellipse (on the transverse plane) with anisotropic expansion (indicated by radial arrows), and a strong magnetic field pointing upward generated by the spectator protons. The reaction plane is defined by the impact parameter direction and the beam direction

2 Early measurements and the background issue

Intensive efforts have been invested to search for the CME in heavy ion collisions at BNL's Relativistic Heavy Ion Collider (RHIC) and CERN's Large Hadron Collider (LHC) [21–23]. Among various observables [24–28], a typically used observable to measure the CME-induced charge separation in heavy ion collisions is the three-point correlator [29],

$$\gamma \equiv \langle \cos(\alpha + \beta - 2\psi) \rangle, \quad (1)$$

where α and β are the azimuthal angles of two particles, and ψ is the angle of the reaction plane (RP, span by the beam and impact parameter directions of the colliding nuclei, see Fig. 2 for an illustration). Charge separation along the magnetic field, which is perpendicular to ψ on average, would yield different values of γ for particle pairs of the same-sign (SS) and opposite-sign (OS) charges: $\gamma_{SS} = -1$ and $\gamma_{OS} = +1$, respectively; the values have opposite signs but equal magnitude.

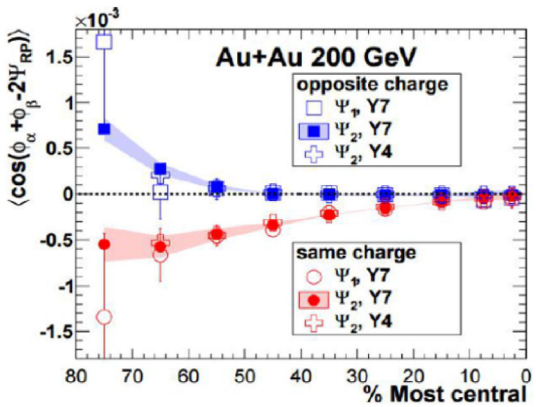

Fig. 3 (Color online) The azimuthal correlator γ measured with the first-order event plane ψ_1 from the ZDCs and the second-order event plane from the time projection chamber (TPC) as functions of centrality in Au + Au collisions at $\sqrt{s_{NN}} = 200$ GeV from STAR. The Y4 and Y7 represent the results from the 2004 and 2007 RHIC runs, respectively. Shaded areas for the results measured with ψ_2 represent the systematic uncertainty of the event plane determination. Systematic uncertainties for the results with respect to ψ_1 are negligible compared to the statistical ones shown. From Ref. [32]

Indeed, signals that are qualitatively consistent with the CME expectations have been observed [25, 30–34]. Figure 3 shows the example results [32] from STAR in 200 GeV Au + Au collisions. Experimentally, the angle ψ is often reconstructed from the azimuthal distribution of the final-state particle density by the fact that the particle density is the largest along the short axis of the collision overlap geometry (see Fig. 2) [35]. This is typically attributed to the hydrodynamic expansion of the high-density collision region, generating an elliptical flow (v_2) [36, 37]. In particular, it is the second harmonic (typically labeled as ψ_2 as in Fig. 3) of the particle density azimuthal distribution, corrected for finite multiplicity resolution [35]. Because of the fluctuations of the nucleon positions in the colliding nuclei, the reconstructed ψ_2 corresponds to the participant plane (PP). It unnecessarily coincides with the RP; however, it fluctuates about the RP event by event [38]. Meanwhile, the RP can be determined more accurately by the spectator neutrons measured by a zero-degree calorimeter (ZDC) [39] (typically labeled as ψ_1, as in Fig. 3) because of a slight side kick they received from the collision [40]. More discussions are presented in Sect. 3.3.

However, background correlations unrelated to the CME exist [41–48]. For example, transverse momentum conservation induces correlations among particles that are enhanced back-to-back pairs [42–46]. Because more pairs are emitted in the RP direction, the net effect of this background is negative, thus dragging the CME-induced $\gamma_{\rm SS}$ and $\gamma_{\rm OS}$, originally symmetric about zero (as illustrated in Fig. 4a), both down in the negative direction (Fig. 4b). This background is, fortunately, independent of particle charges, thus affecting the SS and OS pairs equally, and cancels in the difference,

$$\Delta\gamma \equiv \gamma_{\rm OS} - \gamma_{\rm SS}\,. \tag{2}$$

Experimental investigations have thus focused on the $\Delta\gamma$ observable [21–23]; the CME would yield $\Delta\gamma > 0$.

Unfortunately, mundane physics that differ between SS and OS pairs exist. One such physics is resonance/cluster decays [41–46] that affect OS pairs more significantly than SS pairs (as illustrated in Fig. 4c). This background is positive and arises from the coupling of elliptical anisotropy v_2 of resonances/clusters, and the angular correlations between their decay daughters (nonflow) [41, 42, 45]. Use $\rho \to \pi^+\pi^-$ as an example (Fig. 5). The effect on $\gamma_{\rm OS}$ from the decay of a ρ in the RP direction is identical to a back-to-back pair from the CME in the $\vec{B}$ direction perpendicular to the RP [49]. Because more ρ resonances exist in the RP direction than the perpendicular direction because of the finite v_2 of the ρ, the overall effect on $\gamma_{\rm OS}$ is positive.

There are more sources of particle correlations except that from ρ decays, such as other resonances and jet correlations. We can generally refer to those as cluster correlations [41]. Mathematically, the background can be estimated by

$$\Delta\gamma_{\rm bkgd} \approx \frac{N_{\rm clust.}}{N_\pi^2}\langle\cos(\alpha+\beta-2\phi_{\rm clust.})\rangle v_{2,\rm clust.}\,, \tag{3}$$

where $N_{\rm clust.}$ and N_π are the numbers of clusters and single-charge pions ($N_\pi \approx N_{\pi^+} \approx N_{\pi^-}$), respectively, and $v_{2,\rm clust.} \equiv \langle\cos 2(\phi_{\rm clust.} - \psi)\rangle$ is the v_2 of the clusters [22, 23, 29, 49]. A simple estimate, again using the ρ resonance as an example, indicates that the background magnitude is $\Delta\gamma_{\rm bkgd} \approx \frac{20}{100^2} \times 0.65 \times 0.1 \approx 10^{-4}$ for mid-central Au + Au collisions, comparable to the experimental data in Fig. 3.

3 Innovative methods and new results

Undoubtedly, the early $\Delta\gamma$ measurements [25, 30–34] are dominated by backgrounds. Many proposals and attempts have been realized to reduce or eliminate these backgrounds [24, 25, 49–53]. Examining Eq. 3, it is easy to identify methods to remove backgrounds. One is to measure the $\Delta\gamma$ observable, where the elliptical anisotropy is zero. This has already been exploited in various data analyses [24, 52, 53] and is not a new method. The other is to measure where resonance contributions are small, or can be identified and removed [54, 55]. This has not been explored until recently [56–58]. The following subsections (Sects. 3.1, 3.2) will discuss these two methods with the emphasis on the second one. The third innovative method [59–61], which will be discussed in Sect. 3.3, is not as obvious, but may present the best and most robust method to search for the CME [58].

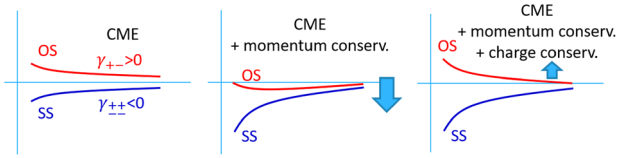

Fig. 4 (Color online) Left: expected CME signals (Eq. 1) for opposite-sign (OS) and same-sign (SS) particle pairs; they have opposite signs but equal magnitude. Center: effect of momentum conservation is negative and equal for OS and SS. Right: effect of local charge conservation (e.g., neutral resonance decays) is positive and only applies to OS

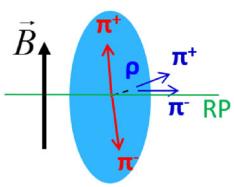

Fig. 5 (Color online) Illustration of the decay $\pi^+\pi^-$ pair from a ρ moving in the RP direction exhibiting the same effect on the γ observable (Eq. 1) as a CME $\pi^+\pi^-$ pair perpendicular to the RP

3.1 Make the anisotropy vanish

This method comprises two variations. The central idea of the first variation is that "round" events with zero elliptical anisotropy ($v_2^{\rm obs}$) exists owing to event-by-event statistical and dynamical fluctuations. This was exploited by STAR [24], where a charge asymmetry observable (similar to $\Delta\gamma$) was analyzed as a function of the observed event-by-event $v_2^{\rm obs}$; both the $\Delta\gamma$ and $v_2^{\rm obs}$ are calculated from the same group of particles (particles of interest, or POI). This is shown in Fig. 6. A clear linear dependence was observed, as expected from the background. The background-suppressed CME signal can be extracted from the intercept at $v_2^{\rm obs} = 0$. With the limited statistics from Run-4 data (taken in the year 2004 by STAR), the extracted intercept is consistent with the zero in the 200 GeV Au + Au collisions [24]. Analysis of higher statistics data from later runs indicates that the intercept is finite [62]. However, the intercept at $v_2^{\rm obs} = 0$ may still contain residual backgrounds because the backgrounds are owing to the nonvanishing $v_{2,\rm clust.}$ of the correlation sources (resonances/clusters) (see Eq. 3), and not the $v_2^{\rm obs}$ measured by the final-state charged hadrons. It was shown by a toy-model resonance simulation [49] that the resonance v_2 is not zero when the event-by-event $v_2^{\rm obs}$ of the final-state hadrons is required to be zero. Even if one could ensure that the event-by-event v_2 of one resonance type is zero, it is nearly impossible to ensure the event-by-event v_2's of all the background sources to be zero. Furthermore, the background in Eq. 3 is proportional to $v_{2,\rm clust.}$ only when $\cos(\alpha+\beta-2\phi_{\rm clust.})$ and $\cos 2(\phi_{\rm clust.}-\psi)$ are factorized. This may not be the case because both depend on the transverse momentum ($p_{\rm T}$) of the cluster [49].

The second variation of the method is to analyze the $\Delta\gamma$ observable of the POI as a function of the flow vector magnitude (q_2) [63] that is calculated not using the POI but the particles from different phase spaces [52, 53]. The q_2 is closely related to v_2, and this method is known as "event-shape engineering (ESE)" [63]. ALICE [52] divided their data in each collision centrality according to q_2 and found the $\Delta\gamma$ to be approximately proportional to the v_2 of the POI; this is consistent with the background contributions. This is shown in Fig. 7. One could fit the data with the linear function in v_2 and extract the possible CME signal by the fit intercept. However, within each relatively wide centrality bin, the magnetic field most probably varies. Thus, ALICE modeled $B(v_2)$ to extract the CME signal. The extracted signal is found to be smaller than 20% of the early, inclusive $\Delta\gamma$ measurement at the 95% conference level [52].

The attractive aspect of this second variation of the method is that it can maintain the magnetic field and vary the event-by-event v_2 [24, 64, 65]. CMS attempts to achieve this using narrow centrality bins [53] such that the extracted CME signal is less model dependent. The CMS results indicate that the CME signal is less than 7% of the inclusive $\Delta\gamma$ at the 95% confidence level [53].

Because the ESE control knob q_2 and the POI are from different phase spaces, a given q_2 cut-bin samples a v_2 distribution of the POI. The extrapolated zero average v_2 of the POI likely corresponds to the zero average v_2 of all particle species, including the CME-background sources of resonances and clusters. This is clearly advantageous over the first variation of the method using the event-by-event $v_2^{\rm obs}$. The disadvantage is that an extrapolation to $v_2 = 0$ is required as the ESE q_2 sampling does not cover the most important $v_2 = 0$ region. A dependence of the backgrounds on v_2 that is not strictly linear would introduce imprecision in the extracted CME signal.

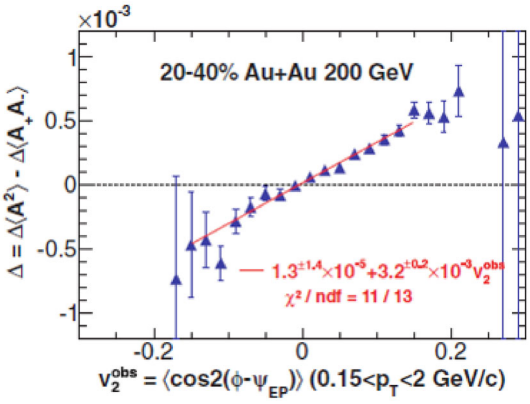

Fig. 6 (Color online) Charge multiplicity asymmetry correlation (Δ) as a function of the event-by-event anisotropy $v_2^{\rm obs}$ in 20–40% Au + Au collisions at $\sqrt{s_{\rm NN}} = 200$ GeV from Run-4 by STAR. Errors are statistical. From Ref. [24]

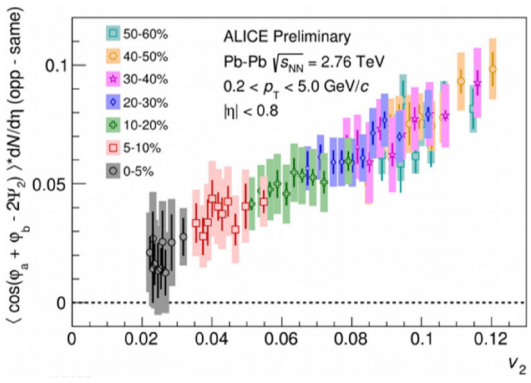

Fig. 7 (Color online) The charged-particle density-scaled azimuthal correlator, $\Delta\gamma \cdot {\rm d}N_{\rm ch}/{\rm d}\eta$, as a function of v_2 for q_2 shape-selected events for various centrality classes in Pb + Pb collisions by ALICE. Error bars (shaded boxes) represent the statistical (systematic) uncertainties [52]

3.2 Identify backgrounds by invariant mass

The particle pair invariant mass ($m_{\rm inv}$) is a typical method to identify resonances. Until recently [54], $m_{\rm inv}$ had not been utilized to investigate the CME $\Delta\gamma$ signal.

The upper panel in Fig. 8 shows the relative OS excess over the SS pion pairs in Run-11 Au + Au collisions from STAR [56–58]. The pions are identified by the TPC and time-of-flight (TOF) detector within pseudorapidity and $p_{\rm T}$ ranges of $|\eta|<1$ and $0.2<p_{\rm T}<1.8$ GeV/c, respectively. The resonance peaks of K_S and ρ are clearly shown. The large increase toward the low-$m_{\rm inv}$ kinematic limit is owing to the acceptance edge effect, where the OS and SS pair acceptance differences of the detector are amplified [58, 66]. The lower panel shows the $\Delta\gamma$ measurement as a function of $m_{\rm inv}$. A clear peak at the K_S mass is observed; a peak at the ρ mass is observable. Most $\pi^+\pi^-$ pair resonances are below $m_{\rm inv}<1.5$ GeV/c^2 ; at higher $m_{\rm inv}$, the resonance contribution can be neglected. The easiest method to remove resonance contributions from $\Delta\gamma$ is, therefore, to restrict the measurements to the large-$m_{\rm inv}$ region. Figure 9 shows the measured $\Delta\gamma$ at $m_{\rm inv}>1.5$ GeV/c^2 , compared to the inclusive $\Delta\gamma$. The large-mass $\Delta\gamma$ is significantly lower by a factor of 20, compared to the inclusive $\Delta\gamma$, and is consistent with zero within a 2σ standard deviation.

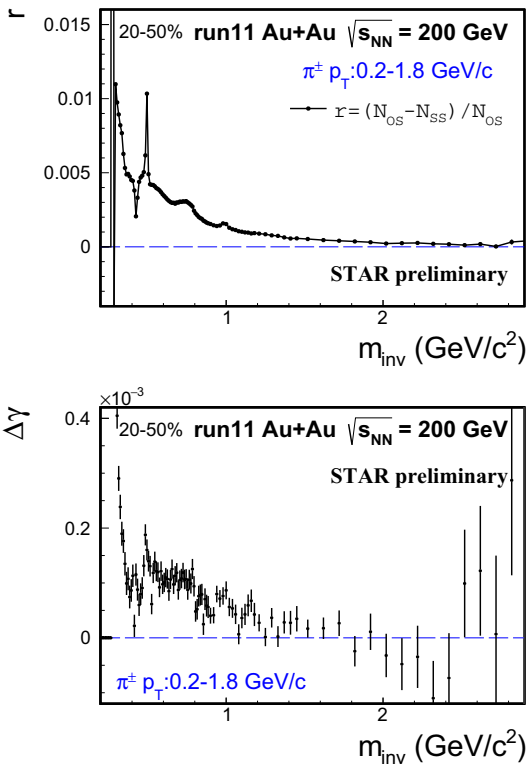

Fig. 8 (Color online) $m_{\rm inv}$ dependences of the relative OS excess over SS pairs (upper) and $\Delta\gamma$ (lower) in 20–50% central Au + Au collisions at $\sqrt{s_{\rm NN}}=200$ GeV from Run-11 by STAR. Errors are statistical [58]

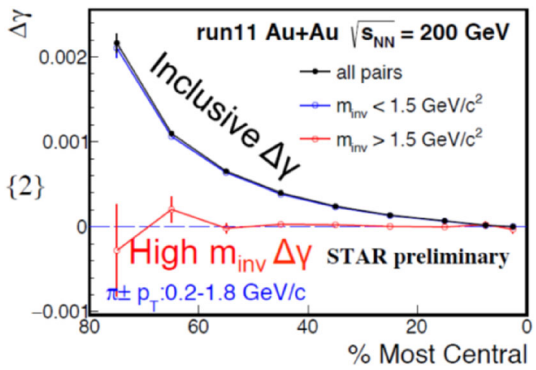

Fig. 9 (Color online) Average $\Delta\gamma$ at large pair mass $m_{\rm inv}>1.5$ GeV/c^2 , compared to the inclusive $\Delta\gamma$, as a function of centrality in 20–50% central Au + Au collisions at $\sqrt{s_{\rm NN}}=200$ GeV from Run-11 by STAR. Errors are statistical [58]

The CME is a low-$p_{\rm T}$ phenomenon and may not be appreciable at high $m_{\rm inv}$, although theoretical calculations suggest that the CME survives at $m_{\rm inv}>1.5$ GeV/c[67]. To extract the CME signal in the low-$m_{\rm inv}$ region, one needs the $m_{\rm inv}$ dependence of the background contribution. STAR used the ESE technique [58], dividing events from each narrow centrality bin into two classes according to the event-by-event q_2 [63]. Because the magnetic fields are approximately equal while the backgrounds differ, the $\Delta\gamma(m_{\rm inv})$ difference between the two classes is a good estimate of the background shape. Figure 10 shows the $\Delta\gamma_A$ and $\Delta\gamma_B$ from such two q_2 classes in the upper panel, and the difference $\Delta\gamma_A-\Delta\gamma_B$ together with the inclusive $\Delta\gamma$ of all events in the lower panel [58].

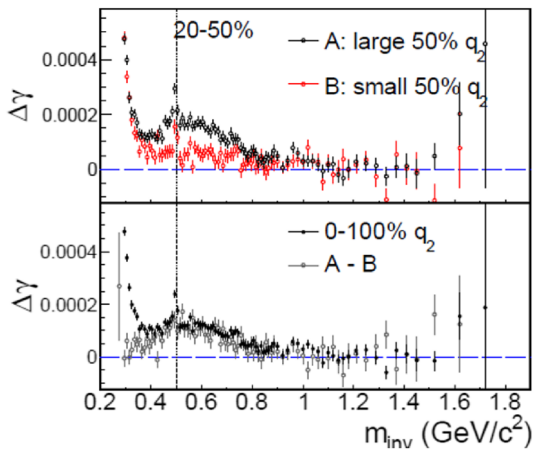

Fig. 10 (Color online) $m_{\rm inv}$ dependences of the $\Delta\gamma$ in large and small q_2 events (upper), and the $\Delta\gamma$ difference between large and small q_2 events together with the inclusive $\Delta\gamma$ (lower) in 20–50% central Au + Au collisions at $\sqrt{s_{\rm NN}}=200$ GeV from Run-16 by STAR. Errors are statistical. From Ref. [58]

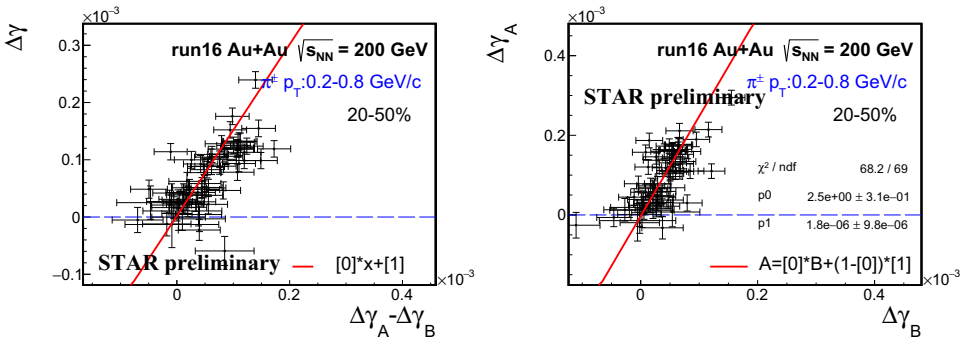

Fig. 11 (Color online) $\Delta\gamma$ versus $\Delta\gamma_A - \Delta\gamma_B$ (left), and $\Delta\gamma_A$ versus $\Delta\gamma_B$ (right) in 20–50% central Au + Au collisions at $\sqrt{s_{\rm NN}} = 200$ GeV from Run-16 by STAR. Each data point in the left (right) panel corresponds to one $m_{\rm inv}$ bin in the lower (upper) panel of Fig. 10; only the $m_{\rm inv} > 0.4$ GeV/c^2 data points are included. Errors are statistical [58]

With the background shape given by $\Delta\gamma_A - \Delta\gamma_B$, the CME can be extracted from a two-component fit to the following form: $\Delta\gamma = k(\Delta\gamma_A - \Delta\gamma_B) + \Delta\gamma_{\rm CME}$. The left panel in Fig. 11 shows $\Delta\gamma$ as a function of $\Delta\gamma_A - \Delta\gamma_B$, where each data point corresponds to one $m_{\rm inv}$ bin in the lower panel of Fig. 10 [58]. Only the $m_{\rm inv} > 0.4$ GeV/c^2 data points are included in Fig. 11 because the $\Delta\gamma$ from the lower $m_{\rm inv}$ region is affected by the edge effects of the STAR TPC acceptance [58, 66]. As shown, a positive linear correlation exists between $\Delta\gamma$ and $\Delta\gamma_A - \Delta\gamma_B$. However, because the same data were used in the measurements of $\Delta\gamma$ and $\Delta\gamma_A - \Delta\gamma_B$, their statistical errors are correlated. To accommodate the statistical errors, one can simply fit the independent measurements of $\Delta\gamma_A$ against $\Delta\gamma_B$, namely by

$$\Delta\gamma_A = b\Delta\gamma_B + (1-b)\Delta\gamma_{\rm CME}, \tag{4}$$

where b and $\Delta\gamma_{\rm CME}$ are the fitting parameters. The right panel of Fig. 11 shows $\Delta\gamma_A$ against $\Delta\gamma_B$, and the fit by Eq. 4 superimposed as the straight line [58]. The straight line superimposed on the left panel of Fig. 11 is the same fit to Eq. 4, converted properly. The parameter b reflects the relative background contribution in the large-q_2 (large-v_2) event class to that in the small-q_2 (small-v_2) event class; further, because the background increases with v_2, the value of b is larger than unity. The CME signal $\Delta\gamma_{\rm CME}$ obtained from the fit is consistent with zero.

In this fit model, unlike the simple ESE method described in Sect. 3.1, the background is not required to be strictly proportional to v_2. Provided that the backgrounds are different for different q_2 event classes, one can extract the background shape as a function of $m_{\rm inv}$. The slope fit parameter in Eq. 4 indicates how good the linearity of the background is against v_2 . The fit model, however, assumes that the CME signal is independent of $m_{\rm inv}$. The good fit quality shown in Fig. 10 indicates that this is a good assumption within the current statistical precision of the data.

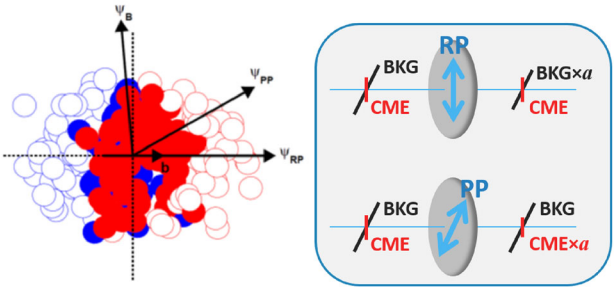

Fig. 12 (Color online) Left: sketch of a heavy ion collision projected onto the transverse plane (perpendicular to the beam direction). $\psi_{\rm RP}$ is the RP (impact parameter, b) direction, $\psi_{\rm PP}$ the PP direction (of interacting nucleons, denoted by the solid circles), and ψ_B the magnetic field direction (primarily from spectator protons, denoted by the open circles together with spectator neutrons). Right: illustration of the "CME-background filter." In a single collision, a CME signal "along" the RP and a background "along" the PP are present. The RP and PP are not the same but differ by an opening angle factor, $a = \langle\cos 2(\psi_{\rm PP} - \psi_{\rm RP})\rangle$. With the "filter" RP, the background is reduced by a factor of a and the CME remains the same, whereas with the "filter" PP, the background remains the same and the CME is reduced by the same factor a

3.3 Compare participant plane and reaction plane

The magnetic field is primarily produced by spectator protons; therefore, its direction is determined by the spectator plane. It is found that the spectator plane nearly coincides with the RP in heavy ion collisions except for highly central collisions [60]. The elliptic flow v_2 is generated by the participants and is therefore determined by the PP [38]. The PP and RP are correlated, but, owing to fluctuations [38], they are not identical. See the illustration in the left panel of Fig. 12. The CME-induced charge separation, driven by the magnetic field [11], will be the strongest along the direction perpendicular to the spectator

plane and will be weaker along the direction perpendicular to the PP. The reduction factor is determined by the opening angle between the two planes and equal to

$$a = \langle \cos 2(\psi_{\mathrm{PP}} - \psi_{\mathrm{RP}}) \rangle. \quad (5)$$

The v_2-induced background, meanwhile, will be the largest in the $\Delta\gamma$ measurement with respect to the PP and will be reduced by the same factor a in the $\Delta\gamma$ measurement with respect to the RP. In other words, the $\Delta\gamma$ measurements with respect to the PP and RP contain different amounts of v_2 backgrounds and CME signals. Thus, the two $\Delta\gamma$ measurements can disentangle the background and the CME signal. This is illustrated in the right panel of Fig. 12; the PP and RP serve as two different filters for the v_2 background and CME signal.

In the experiment, the spectator plane (or closely the RP) can be measured by the ZDCs because of the slight side kick to the spectators in the collision [40]. The PP is, as usual, measured by final-state particles, for example, by the TPC in the STAR experiment [68]. The $\Delta\gamma$ measurements with respect to the RP and PP can readily present the CME signal fraction in the inclusive $\Delta\gamma$ measurement [60]. It is noteworthy that the ZDCs measure only the spectator neutrons [69]; therefore, the measured first-order harmonic plane fluctuates about the RP. Similarly, the final-state particle measurement of the second-harmonic plane is affected by effects other than the elliptic flow [70] and fluctuates about the PP. However, our method does not require a precise determination of the RP and PP [60]. Provided that two experimentally assessable planes exist, onto which the projections of the magnetic field and the elliptic flow are the opposite, our method is robust and is not affected by the uncertainties in assessing the true RP and PP. The plane projection relationship is given by Eq. (5), where the ψ_{PP} and ψ_{RP}, in an experimental data analysis context, should be regarded as the experimentally measured harmonic planes. Figure 13 shows the CME

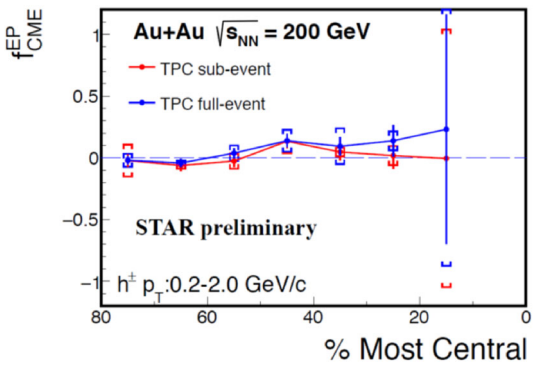

Fig. 13 (Color online) Extracted fraction of potential CME signal as a function of collision centrality in 200 GeV Au + Au collisions by STAR, combining data from Run-11, Run-14, and Run-16. Error bars (horizontal caps) represent statistical (systematic) uncertainties [58]

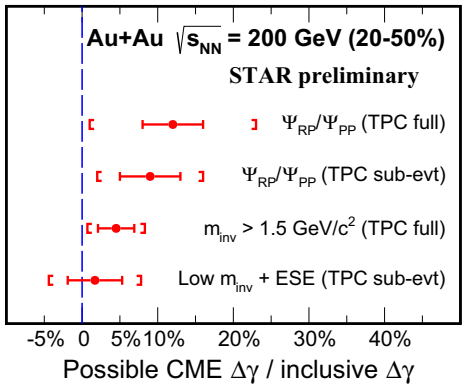

Fig. 14 (Color online) The possible CME signal, relative to the inclusive $\Delta\gamma$ measurement, extracted from the PP–RP comparative measurements and the invariant mass method, in 20–50% central Au + Au collisions at $\sqrt{s_{\mathrm{NN}}} = 200$ GeV by STAR, with a total of 2.5 billion minimum-bias events combining Run-11, Run-14, and Run-16 data. Error bars (vertical caps) represent statistical (systematic) uncertainties. From [58]

signal in terms of its fraction in the inclusive $\Delta\gamma$ measurement as a function of centrality in 200 GeV Au + Au collisions [58]. The two sets of data points correspond to two different acceptance cuts in the analysis. The results are primarily consistent with zero.

4 Discussions and summary

At the LHC, the CMS and ALICE experiments used the ESE method to measure the CME signal without flow background contamination. The CME signal was found to be less than 7% (CMS) [53] and 20% (ALICE) [52] of the inclusive $\Delta\gamma$ measurement at the 95% confidence level.

At the RHIC, two novel methods—invariant mass dependence and comparative PP-RP measurements—have been developed recently. Figure 14 summarizes the current status of the CME signal from STAR in 20–50% central Au + Au collisions at $\sqrt{s_{\mathrm{NN}}} = 200$ GeV [58] using these two methods. The data indicate that the CME signal is small, of the order of a few percent of the inclusive $\Delta\gamma$ measurement, with relatively large errors [58].

In summary, the CME resulted from local $\mathcal{P}$ and $\mathcal{CP}$ violations caused by topological charge fluctuations in QCD. Relativistic heavy ion collisions provided an ideal environment to search for the CME with the strong color gluon field and electromagnetic field. An observation of the CME would confirm several fundamental properties of QCD and solve the strong $\mathcal{CP}$ problem responsible for the matter–antimatter asymmetry in today's universe. Charge-dependent azimuthal correlations with respect to the RP (and PP) were sensitive to the CME, but were contaminated by major physics backgrounds arising from the coupling of

resonance/cluster decays and their elliptic flows (v_2). Intensive theoretical and experimental efforts have been devoted to eliminating those backgrounds and significant progresses have been made in this regard. We herein discussed three novel methods that could potentially measure the background-free CME: ESE, invariant mass ($m_{\rm inv}$) dependence, and comparative measurements with respect to the PP and RP. The current estimates on the strength of the possible CME signal are of the order of a few percent of the inclusive $\Delta\gamma$ values, and 1–2σ standard deviation from zero. It is clear that the experimental challenges in the CME search are daunting, but the important physics warrants continued efforts.

References

1. R.A. Alpher, H. Bethe, G. Gamow, The origin of chemical elements. Phys. Rev. **73**, 803 (1948). https://doi.org/10.1103/PhysRev.73.803
2. A.D. Sakharov, Violation of CP invariance, C asymmetry, and baryon asymmetry of the universe. Pisma Zh. Eksp. Teor. Fiz. **5**, 32 (1967) [JETP Lett. **5**, 24 (1967)] [Sov. Phys. Usp. **34**(5), 392 (1991)] [Usp. Fiz. Nauk. **161**(5), 61 (1991)]. https://doi.org/10.1070/PU1991v034n05ABEH002497
3. M. Dine, A. Kusenko, The origin of the matter: antimatter asymmetry. Rev. Mod. Phys. **76**, 1 (2003). https://doi.org/10.1103/RevModPhys.76.1
4. T. Mannel, Theory and phenomenology of CP violation. Nucl. Phys. Proc. Suppl. **167**, 115 (2007). https://doi.org/10.1016/j.nuclphysbps.2006.12.083
5. R.D. Peccei, H.R. Quinn, CP conservation in the presence of instantons. Phys. Rev. Lett. **38**, 1440 (1977). https://doi.org/10.1103/PhysRevLett.38.1440
6. T.D. Lee, A theory of spontaneous T violation. Phys. Rev. D **8**, 1226 (1973). https://doi.org/10.1103/PhysRevD.8.1226
7. T.D. Lee, G.C. Wick, Vacuum stability and vacuum excitation in a spin 0 field theory. Phys. Rev. D **9**, 2291 (1974). https://doi.org/10.1103/PhysRevD.9.2291
8. P.D. Morley, I.A. Schmidt, Strong P, CP, T violations in heavy ion collisions. Z. Phys. C **26**, 627 (1985). https://doi.org/10.1007/BF01551807
9. D. Kharzeev, R. Pisarski, M.H. Tytgat, Possibility of spontaneous parity violation in hot QCD. Phys. Rev. Lett. **81**, 512 (1998). https://doi.org/10.1103/PhysRevLett.81.512
10. D. Kharzeev, Parity violation in hot QCD: why it can happen, and how to look for it. Phys. Lett. B **633**, 260 (2006). https://doi.org/10.1016/j.physletb.2005.11.075
11. D.E. Kharzeev, L.D. McLerran, H.J. Warringa, The effects of topological charge change in heavy ion collisions: 'event by event P and CP violation'. Nucl. Phys. A **803**, 227 (2008). https://doi.org/10.1016/j.nuclphysa.2008.02.298
12. K. Fukushima, D.E. Kharzeev, H.J. Warringa, The chiral magnetic effect. Phys. Rev. D **78**, 074033 (2008). https://doi.org/10.1103/PhysRevD.78.074033
13. B. Muller, A. Schafer, Charge fluctuations from the chiral magnetic effect in nuclear collisions. Phys. Rev. C **82**, 057902 (2010). https://doi.org/10.1103/PhysRevC.82.057902
14. J. Adams et al., [STAR Collaboration], Experimental and theoretical challenges in the search for the quark gluon plasma: the STAR collaboration's critical assessment of the evidence from RHIC collisions. Nucl. Phys. A **757**, 102 (2005). https://doi.org/10.1016/j.nuclphysa.2005.03.085
15. K. Adcox et al., [PHENIX Collaboration], Formation of dense partonic matter in relativistic nucleus-nucleus collisions at RHIC: experimental evaluation by the PHENIX collaboration. Nucl. Phys. A **757**, 184 (2005). https://doi.org/10.1016/j.nuclphysa.2005.03.086
16. I. Arsene et al., [BRAHMS Collaboration], Quark gluon plasma and color glass condensate at RHIC? The perspective from the BRAHMS experiment. Nucl. Phys. A **757**, 1 (2005). https://doi.org/10.1016/j.nuclphysa.2005.02.130
17. B.B. Back et al., The PHOBOS perspective on discoveries at RHIC. Nucl. Phys. A **757**, 28 (2005). https://doi.org/10.1016/j.nuclphysa.2005.03.084
18. B. Muller, J. Schukraft, B. Wyslouch, First Results from Pb + Pb collisions at the LHC. Ann. Rev. Nucl. Part. Sci. **62**, 361 (2012). https://doi.org/10.1146/annurev-nucl-102711-094910
19. K. Tuchin, Synchrotron radiation by fast fermions in heavy-ion collisions. Phys. Rev. C **82**, 034904 (2010). https://doi.org/10.1103/PhysRevC.82.034904. Erratum: synchrotron radiation by fast fermions in heavy-ion collisions [Phys. Rev. C **82**, 034904 (2010)]. Phys. Rev. C **83**, 039903 (2011) https://doi.org/10.1103/PhysRevC.83.039903
20. D. She, S.Q. Feng, Y. Zhong et al., Chiral magnetic currents with QGP medium response in heavy ion collisions at RHIC and LHC energies. Eur. Phys. J. A **54**, 48 (2018). https://doi.org/10.1140/epja/i2018-12481-x
21. D.E. Kharzeev, J. Liao, S.A. Voloshin et al., Chiral magnetic and vortical effects in high-energy nuclear collisions: a status report. Prog. Part. Nucl. Phys. **88**, 1 (2016). https://doi.org/10.1016/j.ppnp.2016.01.001
22. J. Zhao, Search for the chiral magnetic effect in relativistic heavy-ion collisions. Int. J. Mod. Phys. A **33**, 1830010 (2018). https://doi.org/10.1142/S0217751X18300107
23. J. Zhao, Z. Tu, F. Wang, Status of the chiral magnetic effect search in relativistic heavy-ion collisions. arXiv:1807.05083 [nucl-ex]
24. L. Adamczyk et al., [STAR Collaboration], Measurement of charge multiplicity asymmetry correlations in high-energy nucleus-nucleus collisions at $\sqrt{s_{\rm NN}} = 200$ GeV. Phys. Rev. C **89**, 044908 (2014). https://doi.org/10.1103/PhysRevC.89.044908
25. N.N. Ajitanand, R.A. Lacey, A. Taranenko et al., A New method for the experimental study of topological effects in the quark-gluon plasma. Phys. Rev. C **83**, 011901 (2011)
26. N. Magdy, S. Shi, J. Liao et al., New correlator to detect and characterize the chiral magnetic effect. Phys. Rev. C **97**, 061901 (2018). https://doi.org/10.1103/PhysRevC.97.061901
27. P. Bozek, Azimuthal angle dependence of the charge imbalance from charge conservation effects. Phys. Rev. C **97**, 034907 (2018). https://doi.org/10.1103/PhysRevC.97.034907
28. Y. Feng, J. Zhao, F. Wang, Responses of the chiral-magnetic-effect-sensitive sine observable to resonance backgrounds in heavy-ion collisions. Phys. Rev. C **98**, 034904 (2018). https://doi.org/10.1103/PhysRevC.98.034904
29. S.A. Voloshin, Parity violation in hot QCD: how to detect it. Phys. Rev. C **70**, 057901 (2004). https://doi.org/10.1103/PhysRevC.70.057901
30. B.I. Abelev et al., [STAR Collaboration], Observation of charge-dependent azimuthal correlations and possible local strong parity violation in heavy ion collisions. Phys. Rev. C **81**, 054908 (2010). https://doi.org/10.1103/PhysRevC.81.054908
31. B.I. Abelev et al., [STAR Collaboration], Azimuthal charged-particle correlations and possible local strong parity violation. Phys. Rev. Lett. **103**, 251601 (2009). https://doi.org/10.1103/PhysRevLett.103.251601

32. L. Adamczyk et al., [STAR Collaboration], Fluctuations of charge separation perpendicular to the event plane and local parity violation in $\sqrt{s_{NN}} = 200$ GeV Au + Au collisions at the BNL relativistic heavy ion collider. Phys. Rev. C **88**(6), 064911 (2013). https://doi.org/10.1103/PhysRevC.88.064911
33. L. Adamczyk et al., [STAR Collaboration], Beam-energy dependence of charge separation along the magnetic field in Au + Au collisions at RHIC. Phys. Rev. Lett. **113**, 052302 (2014). https://doi.org/10.1103/PhysRevLett.113.052302
34. B. Abelev et al., [ALICE Collaboration], Charge separation relative to the reaction plane in Pb–Pb collisions at $\sqrt{s_{NN}} = 2.76$ TeV. Phys. Rev. Lett. **110**, 012301 (2013). https://doi.org/10.1103/PhysRevLett.110.012301
35. A.M. Poskanzer, S.A. Voloshin, Methods for analyzing anisotropic flow in relativistic nuclear collisions. Phys. Rev. C **58**, 1671 (1998). https://doi.org/10.1103/PhysRevC.58.1671
36. J.Y. Ollitrault, Anisotropy as a signature of transverse collective flow. Phys. Rev. D **46**, 229 (1992). https://doi.org/10.1103/PhysRevD.46.229
37. U. Heinz, R. Snellings, Collective flow and viscosity in relativistic heavy-ion collisions. Ann. Rev. Nucl. Part. Sci. **63**, 123 (2013). https://doi.org/10.1146/annurev-nucl-102212-170540
38. B. Alver et al., [PHOBOS Collaboration], System size, energy, pseudorapidity, and centrality dependence of elliptic flow. Phys. Rev. Lett. **98**, 242302 (2007). https://doi.org/10.1103/PhysRevLett.98.242302
39. C. Adler, A. Denisov, E. Garcia et al., The RHIC zero-degree calorimeters. Nucl. Instrum. Methods A **499**, 433 (2003). https://doi.org/10.1016/j.nima.2003.08.112
40. W. Reisdorf, H.G. Ritter, Collective flow in heavy-ion collisions. Ann. Rev. Nucl. Part. Sci. **47**, 663 (1997). https://doi.org/10.1146/annurev.nucl.47.1.663
41. F. Wang, Effects of cluster particle correlations on local parity violation observables. Phys. Rev. C **81**, 064902 (2010). https://doi.org/10.1103/PhysRevC.81.064902
42. A. Bzdak, V. Koch, J. Liao, Remarks on possible local parity violation in heavy ion collisions. Phys. Rev. C **81**, 031901 (2010). https://doi.org/10.1103/PhysRevC.81.031901
43. J. Liao, V. Koch, A. Bzdak, On the charge separation effect in relativistic heavy ion collisions. Phys. Rev. C **82**, 054902 (2010). https://doi.org/10.1103/PhysRevC.82.054902
44. A. Bzdak, V. Koch, J. Liao, Azimuthal correlations from transverse momentum conservation and possible local parity violation. Phys. Rev. C **83**, 014905 (2011). https://doi.org/10.1103/PhysRevC.83.014905
45. S. Schlichting, S. Pratt, Charge conservation at energies available at the BNL relativistic heavy ion collider and contributions to local parity violation observables. Phys. Rev. C **83**, 014913 (2011). https://doi.org/10.1103/PhysRevC.83.014913
46. S. Pratt, S. Schlichting, S. Gavin, Effects of momentum conservation and flow on angular correlations at RHIC. Phys. Rev. C **84**, 024909 (2011). https://doi.org/10.1103/PhysRevC.84.024909
47. H. Petersen, T. Renk, S.A. Bass, Medium-modified jets and initial state fluctuations as sources of charge correlations measured at RHIC. Phys. Rev. C **83**, 014916 (2011). https://doi.org/10.1103/PhysRevC.83.014916
48. V.D. Toneev, V.P. Konchakovski, V. Voronyuk et al., Event-by-event background in estimates of the chiral magnetic effect. Phys. Rev. C **86**, 064907 (2012). https://doi.org/10.1103/PhysRevC.86.064907
49. F. Wang, J. Zhao, Challenges in flow background removal in search for the chiral magnetic effect. Phys. Rev. C **95**(5), 051901 (2017). https://doi.org/10.1103/PhysRevC.95.051901
50. A. Bzdak, Suppression of elliptic flow induced correlations in an observable of possible local parity violation. Phys. Rev. C **85**, 044919 (2012). https://doi.org/10.1103/PhysRevC.85.044919
51. F. Wen, J. Bryon, L. Wen et al., Event-shape-engineering study of charge separation in heavy-ion collisions. Chin. Phys. C **42**(1), 014001 (2018). https://doi.org/10.1088/1674-1137/42/1/014001
52. S. Acharya et al., [ALICE Collaboration], Constraining the magnitude of the chiral magnetic effect with event shape engineering in Pb–Pb collisions at $\sqrt{s_{NN}} = 2.76$ TeV. Phys. Lett. B **777**, 151 (2018). https://doi.org/10.1016/j.physletb.2017.12.021
53. A.M. Sirunyan et al., [CMS Collaboration], Constraints on the chiral magnetic effect using charge-dependent azimuthal correlations in *p*Pb and PbPb collisions at the CERN Large Hadron Collider. Phys. Rev. C **97**, 044912 (2018). https://doi.org/10.1103/PhysRevC.97.044912
54. J. Zhao, H. Li, F. Wang, Isolating the chiral magnetic effect from backgrounds by pair invariant mass. arXiv:1705.05410 [nucl-ex]
55. H. Li, J. Zhao, F. Wang, A novel invariant mass method to isolate resonance backgrounds from the chiral magnetic effect. arXiv:1808.03210 [nucl-ex]
56. J. Zhao, [STAR Collaboration], Chiral magnetic effect search in p + Au, d + Au and Au + Au collisions at RHIC. EPJ Web Conf. **172**, 01005 (2018). https://doi.org/10.1051/epjconf/201817201005
57. J. Zhao, [STAR Collaboration], Chiral magnetic effect search in p(d)+Au, Au+Au collisions at RHIC. Int. J. Mod. Phys. Conf. Ser. **46**, 1860010 (2018). https://doi.org/10.1142/S2010194518600108
58. J. Zhao [STAR Collaboration], Measurements of the chiral magnetic effect with background isolation in 200 GeV Au + Au collisions at STAR. arXiv:1807.09925 [nucl-ex]
59. H.J. Xu, X. Wang, H. Li et al., Importance of isobar density distributions on the chiral magnetic effect search. Phys. Rev. Lett. **121**, 022301 (2018). https://doi.org/10.1103/PhysRevLett.121.022301
60. H.J. Xu, J. Zhao, X. Wang et al., Varying the chiral magnetic effect relative to flow in a single nucleus–nucleus collision. Chin. Phys. C **42**, 084103 (2018). https://doi.org/10.1088/1674-1137/42/8/084103
61. H.J. Xu, J. Zhao, X. Wang, et al., Re-examining the premise of isobaric collisions and a novel method to measure the chiral magnetic effect. arXiv:1808.00133 [nucl-th]
62. B. Tu, Charge asymmetry correlations to search for the chiral magnetic effect from beam energy scan by STAR. Kobe, Japan, Sep 27–Oct 3 (2015). https://drupal.star.bnl.gov/STAR/presentations/qm2015/biao-tu
63. J. Schukraft, A. Timmins, S.A. Voloshin, Ultra-relativistic nuclear collisions: event shape engineering. Phys. Lett. B **719**, 394 (2013). https://doi.org/10.1016/j.physletb.2013.01.045
64. S.A. Voloshin, Testing the chiral magnetic effect with central U + U collisions. Phys. Rev. Lett. **105**, 172301 (2010). https://doi.org/10.1103/PhysRevLett.105.172301
65. S. Chatterjee, P. Tribedy, Separation of flow from the chiral magnetic effect in U + U collisions using spectator asymmetry. Phys. Rev. C **92**(1), 011902 (2015). https://doi.org/10.1103/PhysRevC.92.011902
66. L. Adamczyk et al., [STAR Collaboration], Measurements of dielectron production in Au + Au collisions at $\sqrt{s_{NN}} =$ 200 GeV from the STAR experiment. Phys. Rev. C **92**(2), 024912 (2015). https://doi.org/10.1103/PhysRevC.92.024912
67. S. Shi, Y. Jiang, E. Lilleskov et al., Anomalous chiral transport in heavy ion collisions from anomalous-viscous fluid dynamics. Ann. Phys. **394**, 50 (2018). https://doi.org/10.1016/j.aop.2018.04.026
68. M. Anderson, J. Berkovitz, W. Betts et al., The star time projection chamber: a unique tool for studying high multiplicity events at RHIC. Nucl. Instrum. Methods A **499**, 659 (2003). https://doi.org/10.1016/S0168-9002(02)01964-2

69. C. Adler, A. Denisov, E. Garcia et al., The RHIC zero degree calorimeter. Nucl. Instrum. Methods A **470**, 488 (2001). https://doi.org/10.1016/S0168-9002(01)00627-1
70. N.M. Abdelwahab et al., [STAR Collaboration], Isolation of flow and nonflow correlations by two- and four-particle cumulant measurements of azimuthal harmonics in $\sqrt{s_{\mathrm{NN}}} = 200$ GeV Au + Au collisions. Phys. Lett. B **745**, 40 (2015). https://doi.org/10.1016/j.physletb.2015.04.033